Supplementary Material for

Crossover in the pressure evolution of elementary distortions in $RFeO_3$ perovskites and its impact on their phase transition

R. Vilarinho,[1,*] P. Bouvier,[2] M. Guennou,[3] I. Peral,[3] M. C. Weber,[4] P. Tavares,[5] M. Mihalik jr.,[6] M. Mihalik,[6] G. Garbarino,[7] J. Kreisel,[3] A. Almeida,[1] and J. Agostinho Moreira[1,*]

[1]*IFIMUP, Physics and Astronomy Department, Faculty of Sciences, University of Porto, Porto, Portugal.*

[2]*CNRS, Institut Néel, F-38000 Grenoble, France.*

[3]*Materials Research and Technology Department, Luxembourg Institute of Science and Technology, 41, rue du Brill, L-4422 Belvaux, Luxembourg.*

[4]*Department of Materials, ETH Zurich, Vladimir-Prelog-Weg 4, 8093 Zurich, Switzerland*

[5]*Centro de Química, Departamento de Química, Universidade de Trás-os-Montes e Alto Douro, 5000–801 Vila Real, Portugal*

[6]*Institute of Experimental Physics Slovak Academy of Sciences, Watsonova 47, Košice, Slovak Republic.*

[7] *European Synchrotron Radiation Facility, 38043 Grenoble, France.*

*Corresponding author: rvsilva@fc.up.pt

*Corresponding author: jamoreir@fc.up.pt

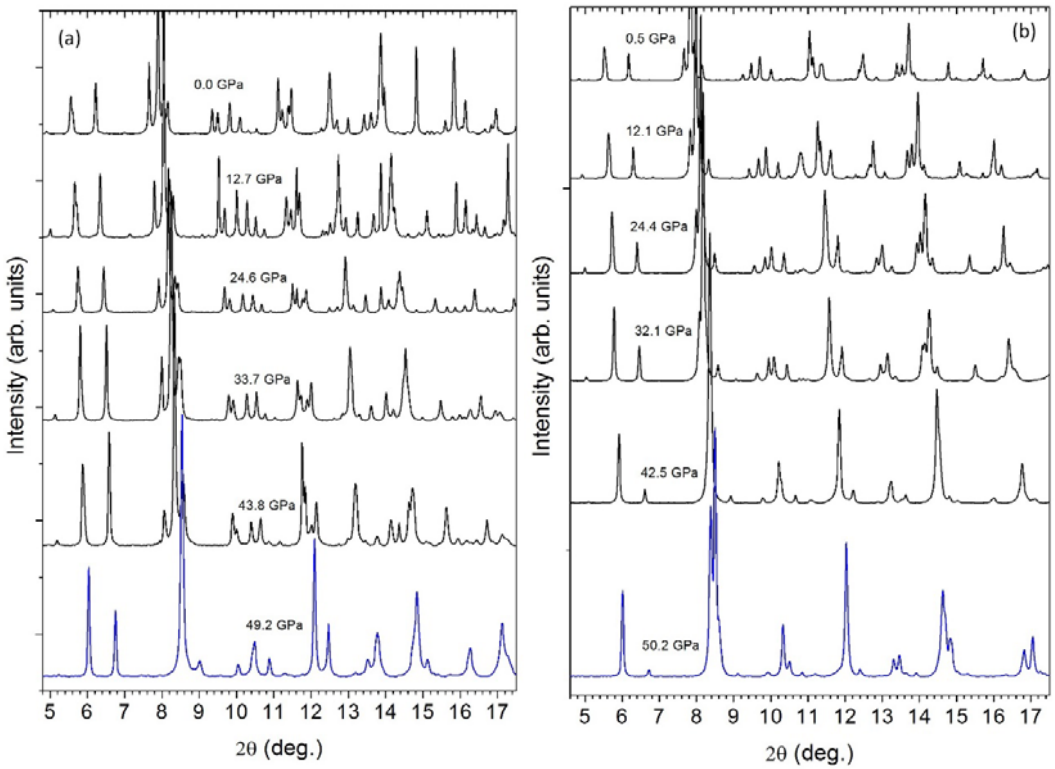

Figure S1. Representative XRD patterns of (a) $TbFeO_3$ and (b) $SmFeO_3$ recorded at different fixed pressures.

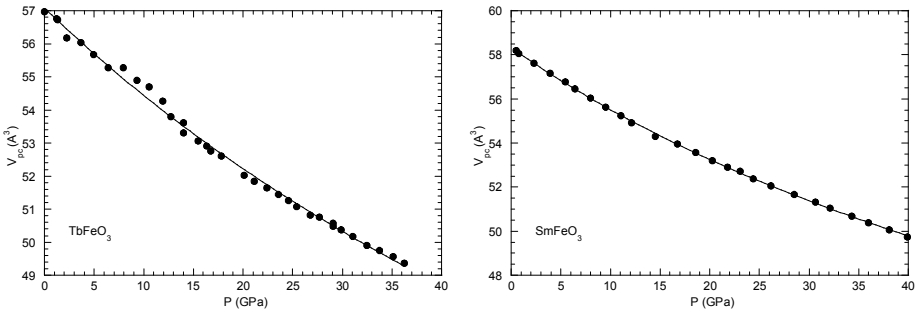

Figure S2. Pseudocubic volume of $TbFeO_3$ and $SmFeO_3$ as a function of pressure, in the orthorhombic phase. The solid line was calculated from the best fit of the third-order Birch-Murnaghan equation of state (Eq. 1) to the experimental data.

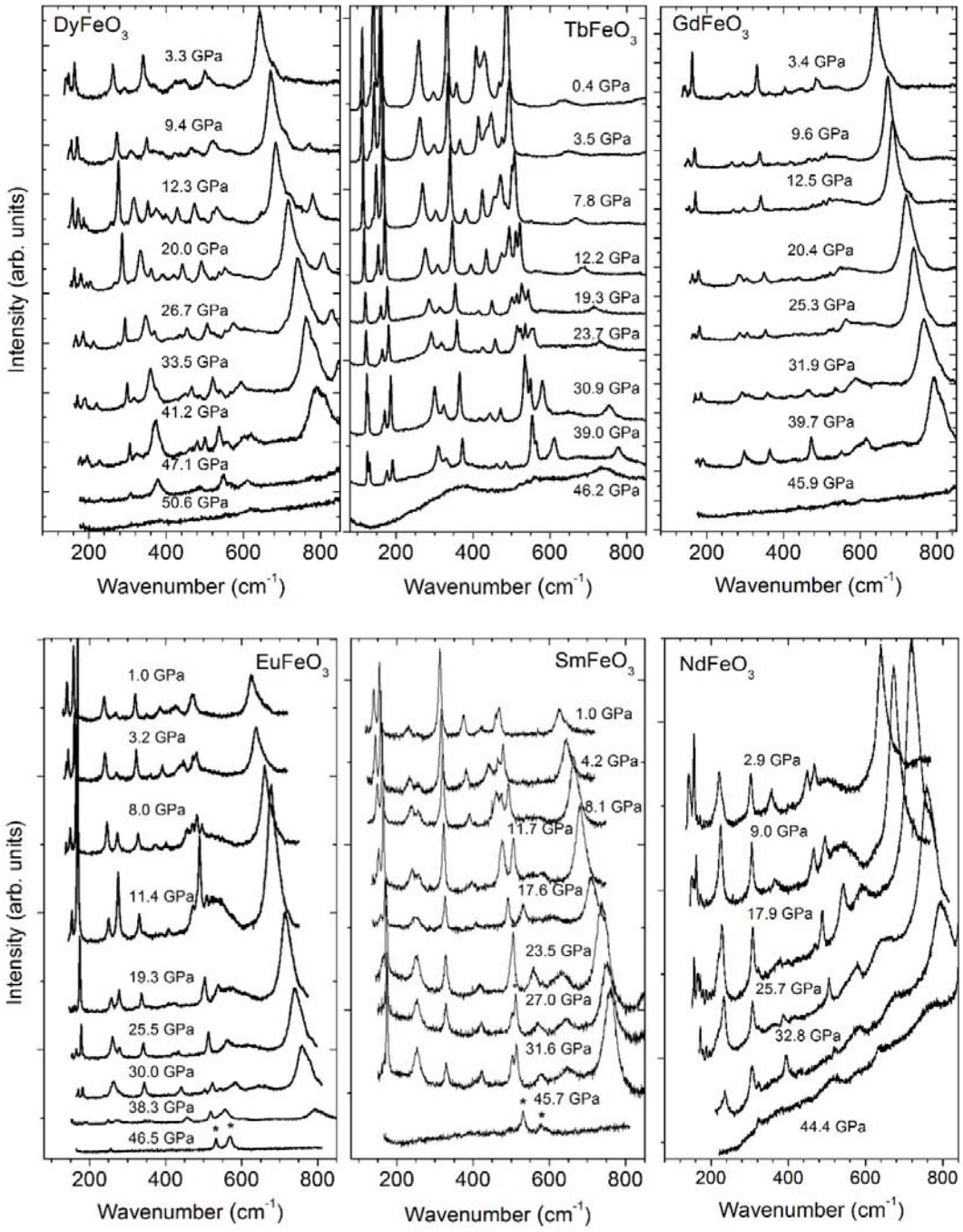

Figure S3. Representative Raman spectra of $DyFeO_3$, $TbFeO_3$, $GdFeO_3$, $EuFeO_3$, $SmFeO_3$ and $NdFeO_3$ recorded at different applied pressures. The peaks marked with * correspond to Raman modes arising from impurity solid phases, which were unintentionally introduced as a minor phase in a helium transmitting medium in the DAC preparation procedure.

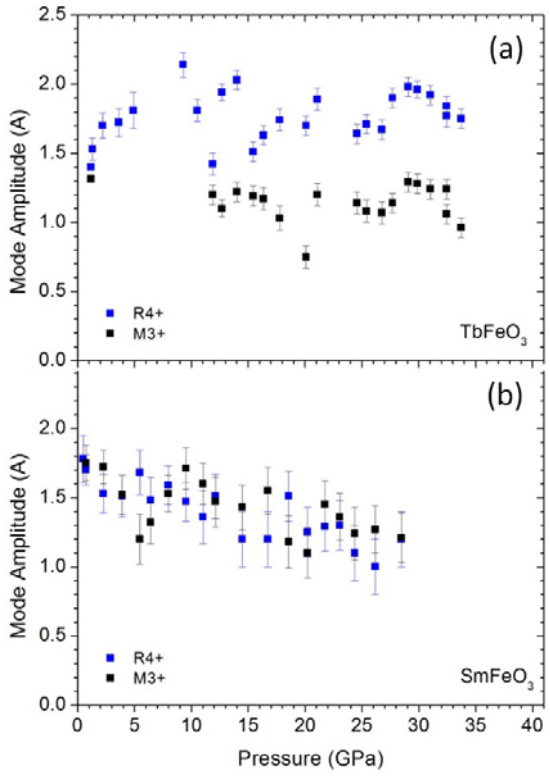

Figure S4. R4+ and M3+ distortions amplitude as a function of pressures obtained by Amplimodes refinement of (a) $TbFeO_3$ and (b) $SmFeO_3$ XRD patterns. For the case of $SmFeO_3$, the smallest distortion (M2+, not presented in this figure) was fixed at the constant value of 0.22 Å to reduce scattering.

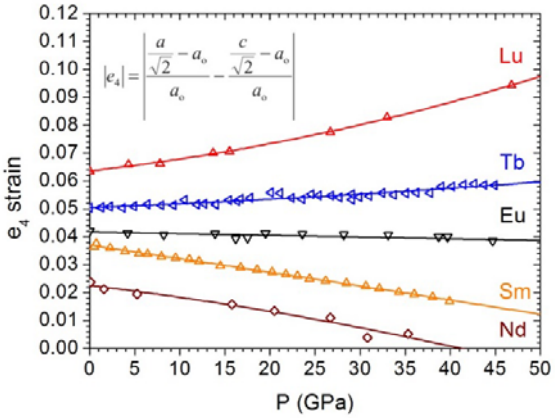

Figure S5. Spontaneous e_4 strain as a function of pressure for different $R FeO_3$. Data of $LuFeO_3$ and $EuFeO_3$ were taken from Ref. 20 and $NdFeO_3$ from Ref. 23.

I. Pressure dependence of the Raman active rotational modes

For $TbFeO_3$ ($SmFeO_3$), the upper shift (down shift) of the frequency of both rotational modes relatively to the universal linear dependence on the BO_6 volume is observed in Figure S6(a) (S6(b)). The observed upper shift (down shift) is a direct consequence of the increase (decrease) of the tilt angles.

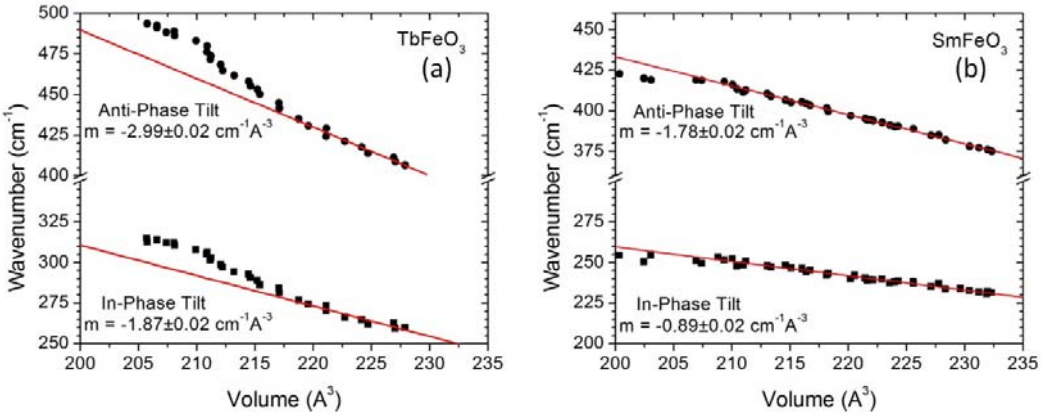

Figure S6. Volume dependence of the frequency of the Raman octahedra rotational modes of (a) $TbFeO_3$ and (b) $SmFeO_3$.

Table I. Pseudo-cubic lattice parameters as a function of pressure $TbFeO_3$ and $SmFeO_3$.

$TbFeO_3$				$SmFeO_3$			
P (GPa)	a_{pc} (Å)	b_{pc} (Å)	c_{pc} (Å)	P (GPa)	a_{pc} (Å)	b_{pc} (Å)	c_{pc} (Å)
1.2	3.9547(3)	3.8162(4)	3.7609(9)	0.5	3.9573(9)	3.852(9)	3.8164(7)
1.3	3.9541(8)	3.8154(5)	3.7600(8)	0.7	3.9569(7)	3.849(8)	3.8115(2)
2.2	3.9428(1)	3.8013(1)	3.7482(8)	2.3	3.9433(9)	3.840(6)	3.8042(3)
3.67	3.9386(2)	3.7982(5)	3.7460(8)	3.9	3.9306(7)	3.830(7)	3.7970(2)
4.9	3.9307(1)	3.7914(5)	3.7362(1)	5.6	3.9197(1)	3.823(1)	3.7893(9)
6.4	3.9225(5)	3.7822(6)	3.7258(8)	6.4	3.9120(7)	3.8154(5)	3.7826(7)
7.9	3.9216(2)	3.7829(6)	3.7263(1)	7.8	3.9005(4)	3.806(5)	3.7747(5)
9.3	3.9147(6)	3.7696(6)	3.7199(6)	9.5	3.8893(7)	3.797(7)	3.7657(7)
10.5	3.8989(7)	3.7585(7)	3.7036(5)	11.0	3.8785(5)	3.790(1)	3.7572(8)
11.9	3.8892(3)	3.7489(7)	3.6936(9)	12.1	3.8699(2)	3.783(6)	3.7515(6)
12.7	3.8867(9)	3.7417(8)	3.6891(4)	14.5	3.8511(2)	3.770(5)	3.7395(3)
14.0	3.8831(2)	3.7426(7)	3.6892(3)	16.7	3.8416(4)	3.763(2)	3.7321(1)
15.4	3.87420	3.7270(1)	3.6744(6)	18.6	3.8306(1)	3.7551(5)	3.7246(1)
16.3	3.8668(2)	3.7252(4)	3.6649(1)	20.2	3.8199(3)	3.747(3)	3.7173(3)
16.7	3.8666(3)	3.72490	3.6664(7)	21.8	3.8107(4)	3.741(1)	3.7115(3)
17.8	3.8650(3)	3.7230(4)	3.6641(3)	23.1	3.8047(3)	3.737(5)	3.7075(7)
20.1	3.8525(5)	3.7060(3)	3.6438(8)	24.4	3.7947(6)	3.7296(5)	3.7014(9)
21.1	3.8490(2)	3.6994(5)	3.6413(3)	26.2	3.7844(4)	3.7232(5)	3.6940(7)
22.4	3.8414(5)	3.6927(9)	3.6408(5)	28.5	3.772(7)	3.7154(5)	3.6857(9)
23.6	3.8341(3)	3.6906(1)	3.6344(7)	30.6	3.7622(3)	3.706(6)	3.6797(1)
24.6	3.8298(2)	3.6891(4)	3.6265(7)	32.1	3.7533(9)	3.701(3)	3.6741(3)

25.4	3.8257(1)	3.6845(5)	3.6219(1)	34.3	3.7417(3)	3.693(5)	3.6670(6)
26.8	3.8191(9)	3.6799(5)	3.6163(8)	36.0	3.7325(3)	3.68(8)	3.660(9)
27.7	3.8171(9)	3.6763(8)	3.6142(7)	38.0	3.7212(2)	3.682(1)	3.653(2)
29.1	3.8114(3)	3.6716(5)	3.6071(1)	39.9	3.7106(1)	3.674(6)	3.6484(6)
29.9	3.8075(5)	3.6686(3)	3.6015(5)	42.5	3.602(2)	3.628(2)	3.641(6)
31.0	3.8027(5)	3.6642(2)	3.5958(5)	44.1	3.590(8)	3.622(8)	3.636(5)
32.5	3.7973(6)	3.6585(3)	3.5900(6)	45.2	3.581(8)	3.613(1)	3.634(2)
33.7	3.7916(1)	3.6553(7)	3.5839(2)	46.4	3.562(1)	3.595(6)	3.627(6)
35.1	3.7872(3)	3.6499(5)	3.5785(3)	47.9	3.542(3)	3.580(6)	3.619(9)
36.2	3.7826(7)	3.6461(7)	3.5732(7)	49.0	3.533(8)	3.568(7)	3.617(3)
37.7	3.7767(1)	3.6435(8)	3.5670(6)	50.2	3.522(6)	3.560(4)	3.613(3)
39.0	3.7724(1)	3.6408(1)	3.5603(8)				
40.2	3.7681(4)	3.636(5)	3.5554(5)				
41.5	3.7637(9)	3.6308(8)	3.5498(8)				
42.6	3.7595(5)	3.6267(3)	3.5448(7)				
43.7	3.7535(5)	3.6218(2)	3.5404(9)				
44.9	3.7475(7)	3.6099(6)	3.5361(2)				
46.2	3.6182(1)	3.5716(2)	3.5387(1)				
47.5	3.5926(4)	3.5603(4)	3.5416(6)				
49.2	3.5632(5)	3.5467(8)	3.5351(2)				
49.8	3.5610(5)	3.5435(5)	3.5320(2)				
50.3	3.5547(8)	3.5414(9)	3.5312(1)				
51.2	3.54790	3.5382(4)	3.5276(7)				
52.3	3.5418(7)	3.5360(7)	3.5245(1)				
53.2	3.5373(2)	3.5342(6)	3.5211(9)				